NANO LETTERS

Letter

pubs.acs.org/NanoLett

Acoustically-Driven Trion and Exciton Modulation in Piezoelectric Two-Dimensional MoS_2

Amgad R. Rezk,[*,†] Benjamin Carey,[‡] Adam F. Chrimes,[‡] Desmond W. M. Lau,[§] Brant C. Gibson,[§] Changxi Zheng,[∥] Michael S. Fuhrer,[∥] Leslie Y. Yeo,[*,†] and Kourosh Kalantar-zadeh[*,‡]

[†]Micro/Nanophysics Research Laboratory, [‡]School of Electrical and Computer Engineering, and [§]Australian Research Council Centre of Excellence for Nanoscale BioPhotonics, RMIT University, Melbourne, Victoria 3001, Australia

[∥]Monash Centre for Atomically Thin Materials, Monash University, Victoria 3800, Australia

Supporting Information

ABSTRACT: By exploiting the very recent discovery of the piezoelectricity in odd-numbered layers of two-dimensional molybdenum disulfide (MoS_2), we show the possibility of reversibly tuning the photoluminescence of single and odd-numbered multilayered MoS_2 using high frequency sound wave coupling. We observe a strong quenching in the photoluminescence associated with the dissociation and spatial separation of electrons−holes quasi-particles at low applied acoustic powers. At the same applied powers, we note a relative preference for ionization of trions into excitons. This work also constitutes the first visual presentation of the surface displacement in one-layered MoS_2 using laser Doppler vibrometry. Such observations are associated with the acoustically generated electric field arising from the piezoelectric nature of MoS_2 for odd-numbered layers. At larger applied powers, the thermal effect dominates the behavior of the two-dimensional flakes. Altogether, the work reveals several key fundamentals governing acousto-optic properties of odd-layered MoS_2 that can be implemented in future optical and electronic systems.

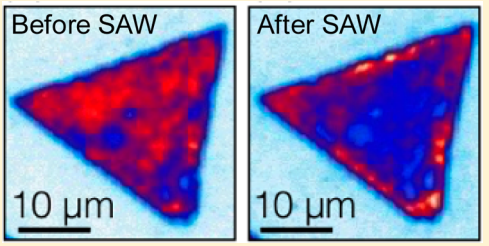

KEYWORDS: *Two-dimensional materials, MoS_2, surface acoustic waves, photoluminescence, exciton, trion, piezoelectricity*

Two-dimensional molybdenum disulfide (2D MoS_2) has attracted increasing attention in recent years due to its fascinating optical,[1] electronic,[2] and piezoelectric properties[3] as well as many of its other remarkable physical and chemical characteristics. The atomic arrangement of 2H-MoS_2 consists of hexagonal planes of S and Mo atoms in a trigonal prismatic structure.[4] Bulk 2H-MoS_2 has an indirect bandgap and weak photoluminescent (PL) properties. However, at a layer thickness of one unit cell MoS_2 undergoes a complete transition from an indirect to a direct bandgap of ∼1.8 eV with energy gaps located at the K and K′ points of the Brillouin zone, producing a strong bandgap PL response.[1] At present, intense research is being undertaken to explore ways to tune these bandgaps, and thus the PL properties of monolayer and few layer MoS_2, for example, via methods such as induced static mechanical straining,[5,6] thermal treatments,[7] electrochemical doping,[8] and electric modulation[9] for use in photovoltaic cells, light-emitting diodes[10] and label-free biosensing,[11] in addition to many other applications.[12]

A very recent discovery is the observation that 2D MoS_2 is by nature piezoelectric if it contains an odd number of layers but not so in even layered configurations. This appears to originate from the opposite orientation of alternating layers in 2H-MoS_2, resulting in an inversion symmetry breaking only in odd-numbered layers, whereas systems with an even number of layers remains centrosymmetric, losing its piezoelectric response. Wu et al.[3] subsequently investigated the piezoelectric properties of one to six layered MoS_2 through continuous stretching and releasing of the flakes with a strain frequency of 0.5 Hz, in which the piezoelectric coupling coefficient was estimated to be ∼5.08% for a single layer and observed to reduce significantly for 3 and 5 layers.

The strong piezoelectricity in MoS_2 opens the possibility of PL modulation and manipulation of excitons and trions through strain-induced electric fields. Here, we exploit a surface acoustic wave (SAW) templates for inducing mechanical displacements in 2D MoS_2 of different number of layers to investigate their piezoelectric effect. While the properties of such acoustic waves on a material's electronic structure and PL has been demonstrated in two-dimensional electron gas (2DEG) systems based on gallium arsenide (GaAs) layered structures,[13] the dissociation of optically generated excitons was only observed in these systems at 4.2 K. Exciton binding energy of GaAs is ∼5 meV[14] so this material does not show any PL at room temperature. Advantageously, the PL for 2D MoS_2 can be seen at room temperature due to its large exciton binding energy of ∼600 meV.[15] The reversible dissociation of the electrons and holes is a useful effect for developing optical and electronic devices in 2D semiconductors as these dissociated charges are dragged along the acoustic waves at the sound speed. As one example, the *e-h* dissociation can be exploited as

Received: July 17, 2015
Revised: December 26, 2015
Published: January 4, 2016

DOI: 10.1021/acs.nanolett.5b02826
Nano Lett. 2016, 16, 849−855

a mechanism in solar cells and electronic junctions based on 2D semiconductors to increase their efficiency. Additionally, the modulated information within the pockets of light that impinges on the 2D flakes can be transferred along the surface and acoustically and/or electrically manipulated. Relatively small electric and acoustic fields are then required to affect the reduced velocity information pockets travel within the 2D materials, as a consequence of the prolonged interaction time of the charges with the fields. Additionally, the information can be modulated within the dissociated charges and be moved along the acoustic waves on the 2D surface to physically transfer the data from one location to another.

High-frequency acoustics have also been used as means to pattern nanowires,[16] deagglomerate carbon nanotube bundles,[17] drive the switching of polymer-dispersed liquid crystal light shutters,[18] and modulate the PL intensity of nanowires[19] and quantum dots (QD).[20] More recently, there has been a recent exploration on the influence of SAWs on quasi-2D MoS_2 materials.[21] However, these polydispersed multilayered quasi-2D materials only showed QD behavior with broad and shifted PL peaks. As a result, the SAW dissociation dynamics has yet to be investigated on atomically thin transition metal dichalcogenides with aspect ratios that produce conditions not seen in the QD domain.

In this work, we use SAWs to introduce mechanical modulation of 2D MoS_2 (as schematically shown in Figure 1a). We show that when the 2D MoS_2 comprises an odd number of layers, it produces a moving electric field due to the inherent piezoelectric properties of this material. Within this moving electric potential, the optically induced excitons and trions can become polarized and dissociate into spatially separated *e-h* quasi-particles. These are then pushed into and stored in potential maxima and minima of the conduction and valence bands as shown in Figure 1b (it is only shown for excitons for brevity). We expect the absence of such modulation in 2D MoS_2 comprising an even number of layers given the lack of inherent piezoelectricity, and therefore no changes in the PL and behavior of *e-h* quasi-particles are expected to be produced (Figure 1c). The aforementioned properties result in a number of observations that will be comprehensively investigated and presented in this paper.

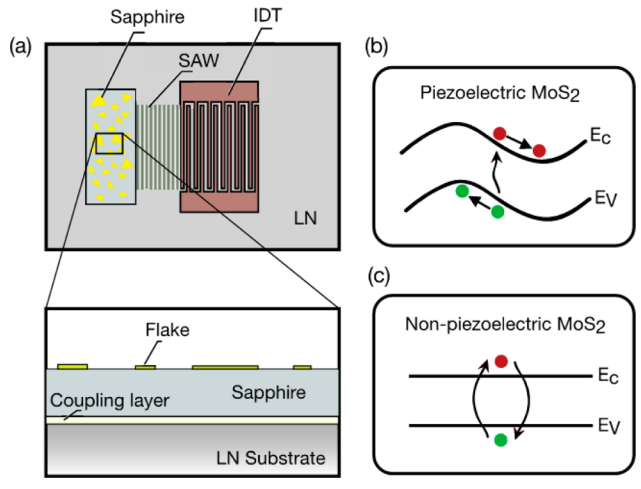

Figure 1. (a) Schematic illustration of the experimental setup comprising the SAW device, which consists of IDT electrodes photolithographically patterned on a lithium niobate (LN) substrate. Applying an alternating electric field at resonance to the IDT gives rise to the SAW that is then transmitted via a fluid coupling layer from the LN substrate into the sapphire substrate on which 2D MoS_2 flakes are grown, as shown from the side view magnification. (b,c) Sketches showing (b) the SAW-induced bandgap modulation (only the exciton case is shown for simplicity) in 2D MoS_2 with an odd number of layers that is inherently piezoelectric, in contrast to (c) the absence of any modulation of the recombination dynamics in 2D MoS_2 with an even number of layers that is nonpiezoelectric.

Specifically, we induce a propagating space periodic strain in 2D MoS_2 using MHz-order frequency Rayleigh SAW generated in a 128° *Y*-cut *X*-propagating $LiNbO_3$ substrate with interdigital transducers possessing a finger width and spacing of 30 μm, the fabrication of which together with the characterization of the SAW are detailed in Methods. The 2D MoS_2 triangular flakes (Figure 2), grown on an atomically smooth sapphire substrate by chemical vapor deposition (CVD), vary in size from a few to several hundreds of microns along the triangular edges and mostly consist of single and up to four layers of MoS_2, assessed using atomic force microscopy (AFM). An example of an AFM image is presented in the figure inset. The flakes are then subject to the SAW vibrational excitation from the $LiNbO_3$ substrate through a conductive fluid (~20 μm thick), which only permitted the propagation of the acoustic wave vibration into the MoS_2 while suppressing the electric field native to the $LiNbO_3$ (see Methods). A range of input powers are employed to the SAW in order to investigate their influence on the PL properties and quasi particles in the different thicknesses of the 2D MoS_2.

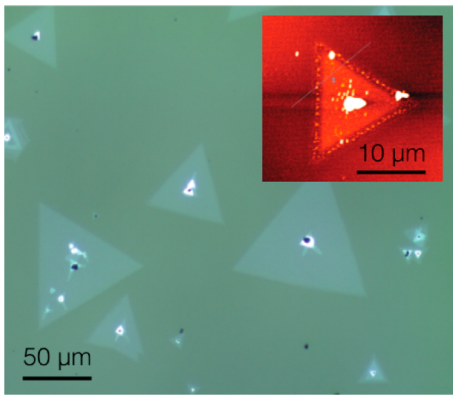

Figure 2. The 10× optical image of the CVD-grown triangular 2D MoS_2 flakes. The inset shows an AFM image of one flake.

PL Map of Single Layer MoS_2. The results from PL mapping across a single layer MoS_2 flake using a custom built laser (532 nm) and spectrometer (details of which are provided in Methods) is presented in Figure 3a. Upon SAW excitation at low input powers up to ~150 mW, quenching in the PL can clearly be observed in the middle of the flake (Figure 3b). Because the flakes are deposited on a sapphire chip and due to the presence of the interstitial fluid couplant with electric field screening effect, they are only acoustically coupled to the underlying $LiNbO_3$ substrate. As a result, the electric component of the SAW is essentially absent in the MoS_2 flake and only the mechanical component coupled into the sapphire substrate, affecting it. Because of the relatively strong inherent piezoelectricity of single layer MoS_2, however, mechanical strain induced by the vibrational displacement produces an electric field in the flake that travels at the acoustic wave velocity of the substrate. After the laser exposure, the

DOI: 10.1021/acs.nanolett.5b02826
Nano Lett. 2016, 16, 849−855

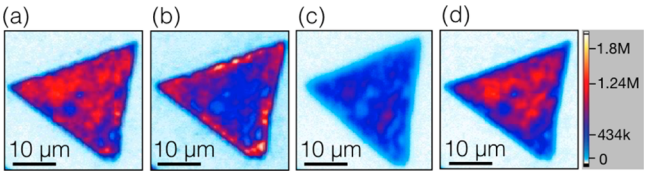

Figure 3. PL map of a single layer MoS_2 flake, showing (a) a uniform PL response under 532 nm laser excitation. (b) Upon SAW excitation, the PL is observed to dramatically decrease within the flake but only in its central regions; the PL is retained along the edges of the flake. (c) Under large SAW excitation powers, heat effects in the sapphire and MoS_2 flakes become dominant and further quenching of the PL, including that at the flake edges, was observed. Finally, the PL was observed to almost recover after the acoustic exposure was discontinued, as shown in (d), wherein some quenching is observed due to autobleaching. The PL intensity scale bar has an arbitrary unit that is consistent across all the images.

optically induced excitons and trions dissociate into spatially separated electrons and holes by the moving electric field within the flake. These electrons and holes remain trapped within the maxima and minima of the potentials in the conductance and valence bands induced by the moving electric field, therefore reducing their probability of recombination and hence quenches the PL (to be discussed in detail subsequently within the text).

The PL quenching upon SAW excitation in the middle of the single layer flakes is in stark contrast to that observed at its edges. As can be seen in Figure 3b, a region with an average width of 2 μm along the flakes' edges exhibits relatively strong PL, suggesting *e-h* recombination in these localized areas. As the samples were kept under ambient conditions for several weeks prior to the experiments, we note that water molecules gradually accumulate and intercalate under the edges of the flakes with time (as seen in the inset of Figure 2), consistent with previous observations.[22] The water molecules, due to their high dielectric constant, then produce a strong screening effect that confines the electric field that, in turn, reduces the potential at the maxima and minima in the conductance and valence bands, resulting in the recombination of the dissociated electrons and holes. As the acoustic waves reflect from all boundaries of the sapphire substrate, the PL bands are seen around all of the edges. As can be seen in Figure 3c, the PL is quenched on the whole surface of the single layer MoS_2 flake at higher SAW applied powers. We ascribe this to heat effects, which will be discussed in the next section.

We also investigate the SAW effect on reversibility of the PL on the MoS_2 flake. As can be seen in Figure 3d, the flake almost regains its PL intensity after the SAW is terminated, where minor quenching is observed possibly due to autobleaching. It asserts that no chemical and/or crystal phase change occurs at the applied SAW powers and that the system is highly reversible. This is further confirmed with Raman scattering measurements for the MoS_2 samples before and after the acoustic exposure, which will be referred to later in the manuscript.

PL Spectra of Single Layer MoS_2 at Different SAW Powers. Figure 4a shows the change in the PL characteristics as a function of the SAW input power for a single MoS_2 layer. In the absence of SAW excitation, the PL spectrum is broad and can be deconvoluted to show the existence of both excitons and trions simultaneously. The trion peak (671 nm) is seen to be larger than the exciton peak (667 nm) due to the doping effects in the sapphire substrate.[23]

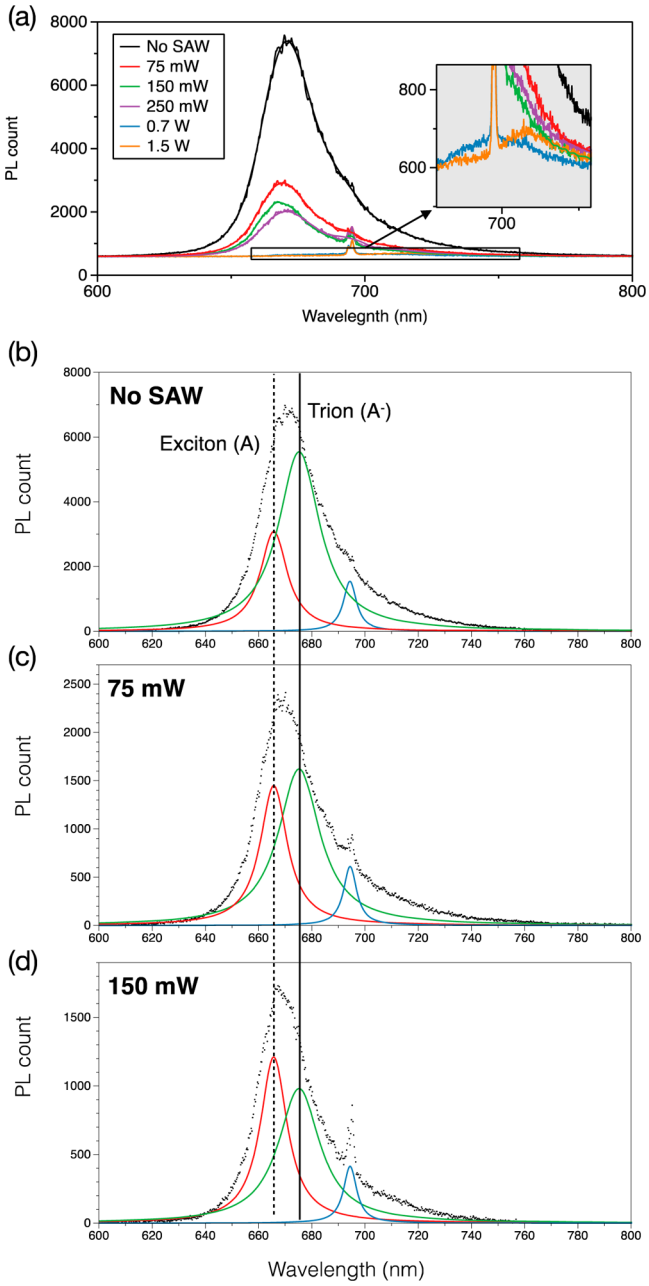

Figure 4. (a) PL spectra of a single layer MoS_2 flake with respect to a range of SAW input powers. At low input powers, strong quenching can be observed together with an apparent shift in the PL peak toward lower wavelengths (higher energies) due to the ionization of trions into excitons by the electric field induced in the flake, triggered as a consequence of its inherent piezoelectricity by the mechanical vibration in the underlying sapphire substrate under SAW exciation. At high SAW input powers, heat generation becomes significant and dominates the dynamics of the bandgap change toward higher wavelengths (lower energies). (b–d) The PL spectra in (a) for single layer MoS_2 for SAW input powers of 0, 75, and 150 mV, respectively, can be deconvoluted to show a systematic increase in the ionization of the trions into excitons as a result of the increasing electric field within the flake, triggered by the larger mechanical displacement of the underlying sapphire substrate as the SAW power is intensified. The peak at ~695 nm is associated with sapphire.

DOI: 10.1021/acs.nanolett.5b02826
Nano Lett. 2016, 16, 849–855

When the SAW is applied at low input powers up to 150 mW, an apparent shift from the trion to exciton peak dominance can be observed. This observation is accompanied by a strong quenching of the PL (~70% of the initial reference value, which can also be seen in the deconvoluted curves in Figure 4b) due to the simultaneous dissociation of the optically generated excitons and trions. The relative ratio of the trion to excition peak intensities reduces from 2.19 to 1.14 when 75 mW power is applied. As the SAW input power increases from 75 to 150 mW, the exciton peak is further enhanced and the ratio decreases to 0.79, indicating the dominance of excitonic quasi-particles. Similar observations have previously been reported and attributed to the ionization of trions into excitons, which is an effect promoted by an intense negative electric field; positive electric fields were not observed to produce any noticeable change.[15] Here, a strong alternating electric field is generated within the piezoelectric single layer MoS_2 flake due to the SAW-induced mechanical field and the negative component of the field plays the role in quasi-particles transition. Given that the temperature of the sapphire substrate and 2D MoS_2 flake rises by only about a maximum of 7 °C, (see Supporting Information Figure S1), thermal effects can be neglected at these low input powers.[7]

To support the hypothesis for the trion to exciton transition, we quantify the energy associated with the electric field induced in a single MoS_2 layer flake as a consequence of its inherent piezoelectricity when the underlying sapphire substrate is subjected to mechanical vibration arising from the SAW excitation. This in turn produces a strain in the flake whose displacement, superimposed on the background displacement of the vibrating sapphire substrate, can be measured using a laser Doppler vibrometer (LDV; Figure 5a,b). To the best of our knowledge, these observations comprise the first visual verification of the piezoelectricity of a single layer MoS_2. As shown in Figure 5b, the mechanical displacements on the flakes are approximately 4 pm larger than the background for an input SAW power of 150 mW. For a flake edge length $L \approx 30\ \mu$m, 2D Young's modulus $E = 130\ \mathrm{Nm}^{-1}$ and induced strain $\varepsilon = 8 \times 10^{-5}$, the resultant electronic energy associated with the induced electric field in the flake, calculated from the corresponding mechanical energy $W_m = L^2E\varepsilon^2/2$ taking into account a piezoelectric conversion efficiency of 5.08%[3] is estimated to be ~130 meV in absolute value, considerably beyond the threshold of the minimum energy for the removal of one electron from a trion, which has been estimated to be around 18 meV.[3] Absorbance measurements for the single layer MoS_2 are also presented in the Supporting Information Figure S2 as further supporting evidence for the trion to excition transition.

Upon increasing the input power (>0.25 W), however, we note that the increase in the mechanical stress in the SAW chip is converted to heat that in turn increases the temperature of the sapphire substrate and the 2D MoS_2 flake substantially. This temperature increase can be as high as 70 °C at the applied input power of 1.5 W (see Figure S1 in the Supporting Information). In addition, the strong quenching of the PL intensity is consistent with that previously reported for PL quenching in both single and few layer MoS_2 under direct heat sources.[7] This is also consistent with the PL red shift of 44 nm in the single layer flake we observe, which can be verified to be a consequence of heating from Varshni's equation. This equation describes the bandgap reduction with temperature

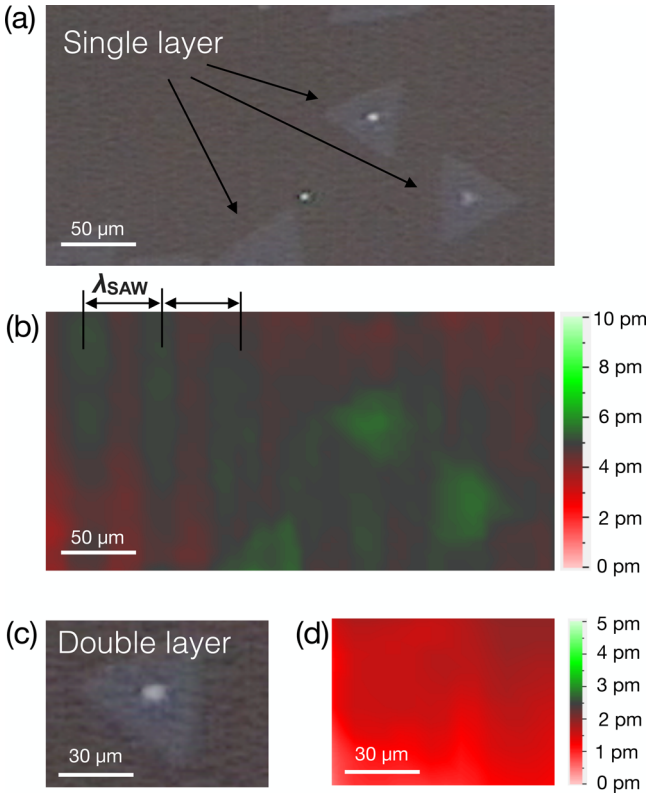

Figure 5. Visual evidence showing the inherent piezoelectricity in 2D MoS_2. The optical image of several single layer MoS_2 flakes is shown in (a) whereas the vibration pattern and intensity measured using the LDV for the same image and corresponding flakes upon acoustic wave excitation are presented in (b). The single layer flakes appear to show larger surface displacements in comparison to the sapphire background due to their intrinsic piezoelectricity. For the two layer MoS_2 flake shown in the optical image in (c), no apparent displacement beyond the background signal associated with the underlying sapphire substrate can be observed in the LDV measurements in (d).

in semiconductors[24] $E_g(T) = E_g(0) - \frac{\alpha T^2}{T+\beta}$. With $E_g(0) = 1.874$ eV, $\alpha = 5.9 \times 10^{-4}$ eV/K, and $\beta = 430$ K,[25] a shift equivalent to an energy difference of 0.13 eV is obtained, which is in exact agreement with Tongay et al.,[7] who also reported a bandgap reduction of 0.13 eV for the ~70 °C temperature increase that we observed. Additional data on the SAW efficiency in quenching the PL of single layer MoS_2 for different laser input and SAW powers are presented in the Supporting Information (Figure S3). Because of the partial trion ionization produced by the SAW, the SAW efficiency in PL quenching is reduced as the laser input power increases. No accompanying change in the composition of the MoS_2 is observed however, as confirmed by the Raman spectra shown in the Supporting Information (Figure S4).

It is of note to consider that Varshni's equation may predict a red shift to be observed at low applied SAW powers (<150 mW), which produces a ~ 7 °C temperature change. In practice, however, no apparent red shift is seen in the PL spectra at these small applied powers. The calculations instead predict that the red shift should be on the order of 1 nm or less, which is comparable with the wavenumber resolution of our PL system. Further, we note that the changes in the trion to exciton peak intensities, at small applied powers, are relatively large and may mask such small thermal effects.

DOI: 10.1021/acs.nanolett.5b02826
Nano Lett. 2016, 16, 849−855

PL Spectra of Two-, Three-, and Four-Layered MoS_2 at Different SAW Powers. Given that the piezoelectric and PL characteristics of 2D MoS_2 is a function of the number of layers it is comprised of,[3,26] we also investigate the influence of the SAW on the PL spectra of 2D MoS_2 with varying number of layers. As shown in Figure 6a, no quenching or shift in the PL is observed when two-layer MoS_2 is excited with low SAW input powers because even-numbered MoS_2 lack inherent piezoelectricity (Figure 1c). This is further verified in Figure 5c,d wherein no vibration displacement on a two-layer flake beyond the background displacement amplitude of the underlying sapphire substrate is evident. There is also little or no quenching in the PL intensity due to residual heating at a higher SAW power of 150 mW (the maximum temperature change is less than 7 °C). The effect of higher temperatures on MoS_2 flakes that cause full PL quenching has been reported elsewhere.[7]

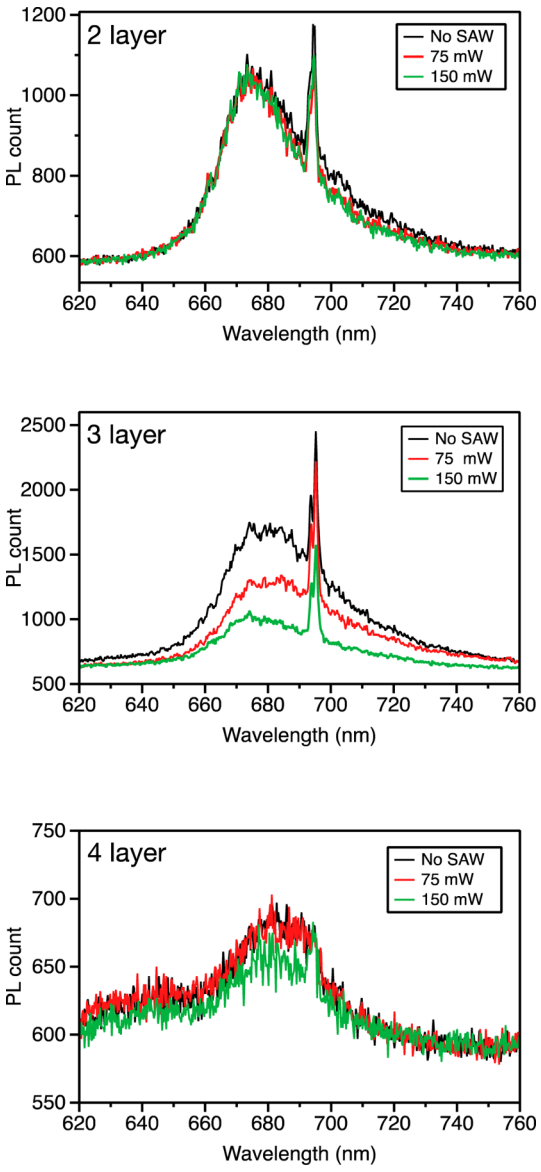

Figure 6. PL spectrum for two-, three-, and four-layered MoS_2 flakes. When the number of layers is even (i.e., two and four layers), as shown in panels b and d, little to no quenching is observed and there is no associated shift in the PL peak because flakes comprising an even number of layers are not inherently piezoelectric. For the three-layered MoS_2 flakes shown in panel c, however, there is significant quenching and a slight shift in the PL spectrum.

In addition to a shift in the PL intensity toward lower wavelengths (higher energies), for three-layered MoS_2 we observe in Figure 6b a return to PL quenching, although this is significantly weaker (38% of the initial reference value) compared to the 70% quenching observed with single layer flakes. This is because MoS_2, consisting of three layers, possesses a weaker piezoelectric electromechanical coupling coefficient compared to its single layer counterpart,[3] thus verifying our hypothesis that the piezoelectricity inherent in odd-numbered layers of 2D MoS_2 layer generates an electric field when it is subject to mechanical modulation that alters its electronic band energies. Finally, as the number of layers is increased to four, only very slight quenching with no shift in the PL is again observed (Figure 6d).

Altogether, important observations are presented regarding the energy values, which are obtained using the piezoelectric equations. According to these piezoelectric measurements and calculations, the applied acoustic wave power induced energies can be on the order of hundreds of millielectronvolts. This presents an opportunity to control the electronic and optical behavior of MoS_2 flakes over a wide energy range using acoustic wave transducers. Considering that the energy difference between the A and B valence bands are ∼150 meV, the energy induced by the piezoelectricity can potentially be used in valleytronic manipulations. Additionally, the piezoelectric effect at lower energies can be used for reversible ionization transformation between trions and excitons for which smaller energies are required.

In summary, large temperature increases under high power acoustic wave excitation are expected to give rise to well-known thermal effects that lead to quenching of the PL in 2D MoS_2. However, high-frequency acoustic excitation of 2D MoS_2 flakes with an odd number of layers, which are inherently piezoelectric, at low to moderate powers are observed to result in dissociated *e-h* quasi-particles in the central flake regions. These dissociated quasi-particles were then transported by the traveling electric field to the screening regions along the flakes' edges where they recombined radiatively. Additionally, there also exists an associated change in the signatures of the PL spectra due to the electric-field induced in the flake by the mechanical vibration of the underlying sapphire substrate due to SAW excitation that promotes the ionization of trions into excitons. This novel possibility for manipulating the electronic band structure in odd-numbered layers of 2D MoS_2 by exploiting its native piezoelectric effect then leads to exciting possibilities for optical and electronic applications of 2D MoS_2 such as optical delays, beam steering, multiplexing, and demultiplexing, among others. The effect can also be used for increasing *e-h* dissociation efficiency in photovoltaic cells.

Methods. *SAW Device Fabrication and Characterization.* Interdigital transducer (IDT) electrodes comprising 40 finger pairs of 10 nm thick chromium used as an adhesive layer and 1.5 μm thick aluminum with a width and gap spacing of 30 μm corresponding to a SAW frequency of 33.3 MHz were patterned on 0.5 mm-thick 4 in. single crystal $LiNbO_3$ piezoelectric wafers using standard photolithographic techniques followed by wet etching. The SAW is then generated by applying an alternating sinusoidal electric field at the resonant frequency to the IDTs using a signal generator (SML01, Rhode & Schwarz Pty. Ltd., North Ryde, NSW, Australia) and

DOI: 10.1021/acs.nanolett.5b02826
Nano Lett. 2016, 16, 849−855

amplifier (ZHL-5W-1, Mini Circuits, Brooklyn, NY). The voltage and current were measured using probes connected to an oscilloscope (Wavejet 332/334; LeCroy, Chestnut Ridge, NY). The fluid couplant consists of pure glycerol.

Mechanical Vibration Visualization. A laser Doppler vibrometer (LDV; UHF-120; Polytec PI, Waldbronn, Germany), was used with a 20× magnification lens and a green laser with 532 nm wavelength.

Sample Preparation. Monolayer MoS_2 single crystals were grown by a sulfur-assisted CVD. The precursors consist of sulfur powder (Sigma-Aldrich, 84683; Sigma-Aldrich Pty. Ltd., Castle Hill, NSW, Australia) and MoS_2 powder (Sigma-Aldrich, 69860; Sigma-Aldrich Pty. Ltd., Castle Hill, NSW, Australia). First, sapphire substrates of Al_2O_3 (0001) were cleaned by 10 min acetone and isopropanol sonication. The sapphire substrates, MoS_2 (0.35 g), and sulfur (0.8 g) were then loaded into three separated quartz crucibles. The growth was performed in a 1 in. diameter quartz tube through which ultrahigh purity argon at atmospheric pressure is flowed. During the growth, the MoS_2 powder and sapphire substrates were loaded at the center and downstream of the furnace, respectively. The sulfur powder was located upstream of the MoS_2 powder and independently heated. The furnace and the sulfur were heated to 940 and 225 °C, respectively, over 30 min. The furnace was then cooled to 500 °C over 10 min, followed by rapid cool down to room temperature. The flow rate of argon was initially kept at 500 sccm. When the furnace temperature reached 500 °C, the flow rate was decreased to 60 sccm. The flow rate was then increased again to 500 sccm when the furnace temperature returned to 500 °C.

PL Measurements. PL mapping was carried out on a custom-built instrument using a monochromatic 532 nm laser (GEM 532, Laser Quantum Ltd., Cheshire, U.K. and WhiteLase, Fianium Ltd., Southampton, U.K.) delivering approximately 200 μW average power to the sample. An air objective (100 0.9NA, Nikon Instruments Inc., Melville, NY) in combination with a 532 nm notch filter was used together with a CCD camera detector (SP2500i and PIXIS100 ExCelon, Princeton Instruments, Trenton, NJ). A spectrometer was used in conjunction to collect in situ PL spectra. The PL spectra were measured when the surface of the device reached a thermal equilibrium after applying SAW.

Raman and Absorbance Measurements. The Raman measurements were conducted using Raman spectroscopy (785 nm, 10 mW laser, 200−2000 cm^{-1} acquisition range; Renishaw plc, Mulgrave, VIC, Australia) while the absorbance measurements were carried out using a UV−vis/NIR microspectrophotometer (20/30 PV, 75W xenon white light source; CRAIC Technologies Inc., San Dimas, CA).

AFM and Optical Characterization. Tapping mode AFM (Digital Instruments D3100, Bruker, Santa Barbara, CA) was used for the flake thickness measurements whereas the optical images were obtained using a materials analysis microscope (DM2500M, Leica Microsystems, North Ryde, NSW, Australia) running in transmission mode.

■ ASSOCIATED CONTENT

Supporting Information

The Supporting Information is available free of charge on the ACS Publications website at DOI: 10.1021/acs.nanolett.5b02826.

Temperature rise in MoS_2 upon SAW exposure, absorbance spectra for different SAW powers, normalized PL measurements for different laser and SAW powers, and Raman spectra. (PDF)

■ AUTHOR INFORMATION

Corresponding Authors

*E-mail: (A.R.R.) amgad.rezk@rmit.edu.au.
*E-mail: (L.Y.Y.) leslie.yeo@rmit.edu.au.
*E-mail: (K.K.-z.) kourosh.kalantar@rmit.edu.au.

Author Contributions

A.R.R., L.Y.Y., and K.K. conceived and designed the experiments. A.R.R. and B.C. performed the photoluminescence experiments with input from D.W.M.L. and B.C.G. The Raman and reflectance measurement were performed by A.F.C. and A.R.R., while C.Z. and M.S.F. fabricated the MoS_2 samples. All authors contributed to the writing of the draft.

Notes

The authors declare no competing financial interest.

■ ACKNOWLEDGMENTS

The authors are thankful for discussions with Dr. Mark J. Holmes at the Institute for Nano Quantum Information Electronics, University of Tokyo. This work was funded in part through an Australian Research Council Discovery Project grants DP140100805, DP150103837 and FL120100038. A.R.R. is grateful for RMIT University for a Vice-Chancellor's Research Fellowship, C.Z. for an Australian Research Council DECRA Grant DE140101555 and L.Y.Y. for a Future Fellowship from the Australian Research Council under Grant FT130100672.

■ REFERENCES

(1) Splendiani, A.; Sun, L.; Zhang, Y.; Li, T.; Kim, J.; Chim, C.-Y.; Galli, G.; Wang, F. *Nano Lett.* **2010**, *10*, 1271.
(2) Yoon, Y.; Ganapathi, K.; Salahuddin, S. *Nano Lett.* **2011**, *11*, 3768.
(3) Wu, W.; Wang, L.; Li, Y.; Zhang, F.; Lin, L.; Niu, S.; Chenet, D.; Zhang, X.; Hao, Y.; Heinz, T. F.; Hone, J.; Wang, Z. L. *Nature* **2014**, *514*, 470.
(4) Mak, K. F.; Lee, C.; Hone, J.; Shan, J.; Heinz, T. F. *Phys. Rev. Lett.* **2010**, *105*, 136805.
(5) Conley, H. J.; Wang, B.; Ziegler, J. I.; Haglund, R. F., Jr; Pantelides, S. T.; Bolotin, K. I. *Nano Lett.* **2013**, *13*, 3626.
(6) Castellanos-Gomez, A.; Roldán, R.; Cappelluti, E.; Buscema, M.; Guinea, F.; van der Zant, H. S.; Steele, G. A. *Nano Lett.* **2013**, *13*, 5361.
(7) Tongay, S.; Zhou, J.; Ataca, C.; Lo, K.; Matthews, T. S.; Li, J.; Grossman, J. C.; Wu, J. *Nano Lett.* **2012**, *12*, 5576.
(8) Wang, Y.; Ou, J. Z.; Balendhran, S.; Chrimes, A. F.; Mortazavi, M.; Yao, D. D.; Field, M. R.; Latham, K.; Bansal, V.; Friend, J. R.; Zhuiykov, S.; Medhekar, N. V.; Strano, M. S.; Kalantar-zadeh, K. *ACS Nano* **2013**, *7*, 10083.
(9) Liu, Q.; Li, L.; Li, Y.; Gao, Z.; Chen, Z.; Lu, J. *J. Phys. Chem. C* **2012**, *116*, 21556.
(10) Wang, Q. H.; Kalantar-Zadeh, K.; Kis, A.; Coleman, J. N.; Strano, M. S. *Nat. Nanotechnol.* **2012**, *7*, 699.
(11) Sarkar, D.; Liu, W.; Xie, X.; Anselmo, A. C.; Mitragotri, S.; Banerjee, K. *ACS Nano* **2014**, *8*, 3992.
(12) Li, H.; Wu, J.; Yin, Z.; Zhang, H. *Acc. Chem. Res.* **2014**, *47*, 1067.
(13) Rocke, C.; Zimmermann, S.; Wixforth, A.; Kotthaus, J. P.; Böhm, G.; Weimann, G. *Phys. Rev. Lett.* **1997**, *78*, 4099.
(14) Bastard, G.; Mendez, E. E.; Chang, L. L.; Esaki, L. *Phys. Rev. B: Condens. Matter Mater. Phys.* **1982**, *26*, 1974.

DOI: 10.1021/acs.nanolett.5b02826
Nano Lett. 2016, 16, 849−855

(15) Mak, K. F.; He, K.; Lee, C.; Lee, G. H.; Hone, J.; Heinz, T. F.; Shan, J. *Nat. Mater.* **2012**, *12*, 207.
(16) Chen, Y.; Ding, X.; Steven, L. S. C.; Yang, S.; Huang, P. H.; Nama, N.; Zhao, Y.; Nawaz, A. A.; Guo, F.; Wang, W.; Gu, Y.; Mallouk, T. E.; Huang, T. J. *ACS Nano* **2013**, *7*, 3306−3314.
(17) Miansari, M.; Qi, A.; Yeo, L. Y.; Friend, J. R. *Adv. Funct. Mater.* **2015**, *25*, 1014−1023.
(18) Liu, Y. J.; Ding, X.; Lin, S. C. S.; Shi, J.; Chiang, I. K.; Huang, T. J. *Adv. Mater.* **2011**, *23*, 1656−1659.
(19) Hernández-Mínguez, A.; Mo ller, M.; Breuer, S.; Pfu ller, C.; Somaschini, C.; Lazic, S.; Brandt, O.; García-Cristóbal, A.; de Lima, M. M., Jr; Cantarero, A. *Nano Lett.* **2012**, *12*, 252.
(20) Fletcher, N. E.; Ebbecke, J.; Janssen, T. J. B. M.; Ahlers, F. J.; Pepper, M.; Beere, H. E.; Ritchie, D. A. *Phys. Rev. B: Condens. Matter Mater. Phys.* **2003**, *68*, 245310.
(21) Rezk, A. R.; Walia, S.; Ramanathan, R.; Nili, H.; Ou, J. Z.; Bansal, V.; Friend, J. R.; Bhaskaran, M.; Yeo, L. Y.; Sriram, S. *Adv. Opt. Mater.* **2015**, *3*, 888.
(22) Zheng, C.; Xu, Z.-Q.; Zhang, Q.; Edmonds, M. T.; Watanabe, K.; Taniguchi, T.; Bao, Q.; Fuhrer, M. S. *Nano Lett.* **2015**, *15*, 3096.
(23) Buscema, M.; Steele, G. A.; van der Zant, H. S.; Castellanos-Gomez, A. *Nano Res.* **2014**, *7*, 561.
(24) Varshni, Y. *Physica* **1967**, *34*, 149.
(25) Korn, T.; Heydrich, S.; Hirmer, M.; Schmutzler, J.; Schüller, C. *Appl. Phys. Lett.* **2011**, *99*, 102109.
(26) Mak, K. F.; Lee, C.; Hone, J.; Shan, J.; Heinz, T. F. *Phys. Rev. Lett.* **2010**, *105*, 136805.

DOI: 10.1021/acs.nanolett.5b02826
Nano Lett. 2016, 16, 849−855